Attosecond Optical Switching

Mohammed Hassan (mohammedhassan@email.arizona.edu)
University of Arizona https://orcid.org/0000-0002-9669-534X
Dandan Hui
University of Arizona
Husain Alqattan
University of Arizona https://orcid.org/0000-0002-1667-7038
Simin Zhang
Ohio State University
Vladimir Pervak
Ludwig Maximilian University
Enam Chowdhury
Ohio State University

Article

Keywords:

Posted Date: August 4th, 2022

DOI: https://doi.org/10.21203/rs.3.rs-1232650/v2

Abstract

Modern electronics are founded on switching the electric signal by radio frequency (RF) electromagnetic fields on the nanosecond timescale, limiting the information processing to the gigahertz speed. Recently, optical switches have been demonstrated using terahertz and ultrafast laser pulses to control the electric signal and enhance the switching speed to the picosecond and a few hundred femtoseconds time scale. Here, we exploit the reflectivity modulation of the fused silica dielectric system in a strong light field to demonstrate the optical switching (ON/OFF) with attosecond time resolution. Moreover, we present the capability of controlling the optical switching signal with complex synthesized fields of ultrashort laser pulses for data binary encoding. This work paves the way for establishing optical switches and light-based electronics with petahertz speeds, several orders of magnitude faster than the current semiconductor-based electronics, opening a new realm in information technology, optical communications, and photonic processor technologies.

Introduction

The strong light field interaction with the atomic system in the gas phase enabled the generation of the attosecond XUV bursts by the means of high-harmonic generation (HHG)[1,2]. This advancement allowed to study and control of the electron motion induced by synthesized light fields[3,4]. A revolution milestone was achieved by exploiting the strong field interaction and generating XUV pulses by the HHG in bulk solids[5]. The development of attosecond XUV[6–8], and attosecond all-optical spectroscopic measurements[9,10] provided an access to study and control the charge carrier dynamics and the optical properties of the condensed matter. For instance, the strong ultrafast laser pulses have been used to induce phase transition in dielectric material[6–14]. The charge carriers are excited from the valance band to the conduction band in the dielectric via multiphoton excitation[14]. Then, the excited electrons in the conduction band move in the reciprocal space by acquiring a time-dependent momentum from the driving field[6,9,10,14,15]. Hence, the electrons are accelerated and decelerated following the shape of the driver field's vector potential, causing an instantaneous modulation in the electronic structure of the dielectric system[9,15–17]. Consequently, the dielectric undergoes an instantaneous phase transition, causing alternations in the dielectric constant and the optical properties of the system due to the strong polarizability[12,18]. Hence, the reflectivity modulation of the fused silica following the driver field[14] enables the control of the material and its optical properties in real-time. Earlier, this interaction has been exploited for sampling the light field of laser pulses, demonstrating the capability of electron motion control, and determining the relative electronic delay response in different dielectric systems[9,10]. In this work, we demonstrate the attosecond optical switching exploiting the oscillation of the dielectric material reflectivity from maximum to minimum in a half field-cycle time scale as illustrated in Fig. 1. Accordingly, the reflected light signal is switching from ON to OFF with sub-femtosecond resolution. This demonstration paves the way to establish ultrafast optical switches with petahertz (1.1 PHz) speeds beyond the state-of-the-art advancement of demonstrated optical switching[19–31]. Moreover, using

complex synthesized light field waveforms to alter the reflectivity of the dielectric enables one to control the switching signal and allows the digital binary encoding with the petahertz speed.

Results

Transient reflectivity switching in sub-femtosecond time scale.

In our experiment, we use a synthesized light waveform generated by the attosecond light field synthesizer (ALFS)[32] (pulse duration = 2.7 fs) with a nominal carrier wavelength = 550 nm to modify the fused silica reflectivity, which is probed by another weak light field (probe pulse), as explained in the Method section. The reflected probe beam spectrum is recorded as a function of the time delay between the pump and probe pulses (Fig. 1). The measured spectrogram (average of three scans) —depicted in Fig. 2a—shows the reflected probe beam (off the fused silica front surface) spectrum in the real-time. The reflectivity modulation is frequency and time dependent which is distinctly observed by subtracting the reflected probe spectrum in the absence of the driver field as shown in the spectrogram in Fig. 2b. Hence, the reflectivity switches from maximum (ON) to a minimum (OFF) in sub-femtosecond (900 as) time scale. The integration of the measured spectra amplitude as a function of time delay—total reflectivity modulation (TRM) trace (Fig. 2c) —gives an access to the vector potential, and the driver field (Extended Data Fig. 1)[9].

At τ=0 fs, the fused silica experiences a phase transition, and the reflectivity increases by ~ 25 (reflected spectrum of the probe beam, in this case, is shown in the red line in Fig. 2d) with respect to the reflectivity of the fused silica in the equilibrium state (reflected spectrum with no field effect shown in the black line in Fig. 2d). In contrast, at τ=0.9 fs, the reflectivity reduces by ~21 %(blue line in Fig. 2d). Hence, the reflectivity changes by a total value of ~45% in a half-cycle time scale representing the switching intensity resolution. Moreover, the measured reflected spectra in Fig. 2d show that the strong field-induced phase transition of the fused silica is reversible following the driver field oscillations direction. Note, the transmission signal of the dielectric system is also varying in the strong field, although, the transmitted light suffers nonlinear propagation and dispersion effects. Therefore, the study of the transmitted light signal is complicated, and does not solely reflect the phase transition dynamics of the system.

Discussion

The ultrafast reflectivity switching presented in Fig. 2 is due to the novel ultrafast material modification controlled by intense synthesized light field in real-time. The first step for proving and understanding the underlying physics of the frequency dependent reflectivity switching in real time is to extract the modulated material reflectivity due to the strong light field interaction. This can be obtained by dividing the reflected probe pulse spectrum (black curve in Fig. 2d) by the intrinsic reflectivity of fused silica, then, deconvolute the result from the measured spectrogram in Fig. 2a. The obtained spectrogram, plotted in Fig. 3a, represents the transient reflectivity change of the fused silica material induced by the strong field of the driver pulse in frequency and time domains. This transient material modification (Fig. 2a and b)

happens in a frequency range far from its higher harmonics spectral range, indicating that the observed reflectivity modulation (in Fig. 2a and b) is not a result of the spectral interference between the high harmonic generation frequencies[33].

From Fig. 3a, we extracted the average amplitude of the reflectivity oscillation at different frequencies and plotted it in the blue line in Fig. 3b. The offset values of the reflectivity modulation as a function of frequency are plotted in the red curve. Each value at a particular frequency corresponds to the offset from zero point of the temporal oscillation, whereas the amplitude values determine how strong the reflectivity oscillations will be as a function of pump-probe time delay for that specific frequency. In addition, the reflectivity of fused silica in the equilibrium state (no influence of the pump pulse) is plotted in the black line. Comparing the frequency oscillation (Fig. 3b) to the spectrum of pump pulse in Fig. 2d (black line), we can observe that the reflectivity peaks do not overlap with the spectrum intensity peaks of the pump pulse, proving that the observed reflectivity modulations seen in our experiment are not due to the interference between the probe and pump pulses. Furthermore, the observed reflectivity oscillations (Fig. 2a,b and Fig. 3a) at any particular frequency are distinct and have steady amplitudes within a time delay range much longer than the pulse's coherence time[34], indicating that again this modulation is not induced due to the conventional interference between the pump and probe pulses.

Moreover, it is clear in Fig. 2a and b and Fig. 3a that for each frequency the reflectivity is oscillating in a periodic oscillation in time associated with that frequency. Also, the oscillation amplitude is controlled by the proximity to an individual resonance frequency in the excited dielectric permittivity induced by the intense pump field. Thus, such ultrafast reflectivity switching can be explained by the interference of the bound-electron resonances, which causes a transient modification of the fused silica dielectric constant (ϵ), refractive index, and its reflectivity in the strong field.

The reflectivity modulation of the dielectric system in a strong field can be expressed as

$$R_m(\omega) = \frac{[1 - n(\omega)]^2 + \kappa^2(\omega)}{[1 + n(\omega)]^2 + \kappa^2(\omega)}$$

1

where $\tilde{n} = \pm\sqrt{\tilde{\epsilon}_r} = n(\omega) + i\kappa(\omega)$ is the refractive index, $\tilde{\epsilon}_r$ is the relative permittivity. For a particular frequency ω_0, the electric fields of pump and probe pulses in the time domain can be expressed as

$$E_{pump} = A_0 e^{i\omega_0 t}$$

2

$$E_{pro} = A_1 e^{i\omega_0 (t + N\Delta t)}$$

3

where A_0 and A_1 are the electric field amplitudes of the pump and probe pulses, respectively. In our experiment $A = A_0/A_1\tilde{1}0$. Δt is the time delay step (100 as), $N\Delta t$ denotes the Nth delay step.

After Fourier transformation, we can write Eqs. 2 and 3 in the spectral domain as

$$\tilde{E}_{pump} = A_0\delta(\omega - \omega_0)$$

4

$$\tilde{E}_{pro} = A_1\delta\left(\omega - \omega_0\right)e^{i\omega N\Delta t}$$

5

and,

$$\frac{\tilde{E}_{pump}}{\tilde{E}_{pro}} = Ae^{-i\omega N\Delta t}$$

6

.

Assuming that the material polarizability, modified by the strong field interaction, affects the propagation of the probe pulse, so the electric field of the probe pulse can be expressed as

$$\nabla\tilde{E}_{pro} = -\omega^2\mu_0\left(\epsilon_0\tilde{E}_{pro} + \tilde{P}_{pump} + \tilde{P}_{pro}\right) = -\omega^2\mu_0\epsilon_0\tilde{E}_{pro}\left(1 + \chi_1\prime + \chi_2\prime\right)$$

$$= -\omega^2\mu_0\epsilon_0\tilde{\epsilon}_{\mathrm{r}}\tilde{E}_{pro}$$

7

where

$$\tilde{\epsilon}_{\mathrm{r}} = 1 + \chi_1\prime + \chi_2\prime$$

8

$$\chi_1' = Ae^{-i\omega N\Delta t}\omega_p^2\sum\nolimits_{k=1,2,\ldots}\frac{f_k}{{\omega_{0,k}}^2 - \omega^2 - i\omega\Gamma_k}$$

9

$$\chi_2' = \omega_p^2\sum\nolimits_{j=1,2,\ldots}\frac{f_j}{{\omega_{0,j}}^2 - \omega^2 - i\omega\Gamma_j} + C$$

10

where μ_0 and ϵ_0 are the permeability and permittivity in vacuum. $\tilde{P}_{pump}$ is the pump-induced material polarization coupled to $\tilde{P}_{pro}$, whereas the latter is the material polarization caused by the probe pulse (note, the intensity of the probe pulse is too weak to induce polarizability change in the system). Eqs. 9 and 10 show that the susceptibility $\chi_1\prime$ (or $\chi_2\prime$) corresponding to $\tilde{P}_{pump}$ (or $\tilde{P}_{prop}$) can be expressed as a combination of multiple Lorentz resonators upon the pump excitation, where $\omega_{0,j}$, Γ_j, and f_j(or $\omega_{0,k}$, Γ_k, and f_k) are the natural frequency, damping rate, and strength of the jth (k^{th}) resonator. C is a constant that represents the effect of resonances far from the spectrum range of interest. $\omega_p^2 = \frac{e^2 n_e}{m\epsilon_0}$ is the square of the plasma frequency, m is the free electron mass. Here, we assume one active electron per molecule in the fused silica, $n_e = 2.2 \times 10^{28}$ m^{-3}.

Accordingly, we utilized Eqs. 9 and 10 to simulate the experimentally measured reflectivity modulation spectrogram of fused silica (shown in Fig. 2a) using our pump pulse field (which is shown in Supplementary Information Fig. S1). The simulation results of the measured spectrograms (Fig. 2a and b) can capture all the measured reflectivity modulation features, as shown in Fig. 3c and d, respectively, by considering the spectral phase of the pump pulse, as explained in the Supplementary Information. The obtained calculated spectrograms, shown in Fig. 3c and d, are in good agreement (Standard deviation = 1.37% and 2.1%) with the measured spectrogram in Fig. 2a, b. The fitting parameters for $\chi_2\prime$ and $\chi_1\prime$, are listed in Table 1 and Table 2 (Supplementary Information).

Based on the experiment and theoretical results, the observed ultrafast reflectivity switching of fused silica can be attributed to the multiphoton resonances in the dielectric permittivity of the fused silica excited by our *unique* high-intensity and broadband near-single-cycle pump pulse. The novelty in our pump pulse is that it has strong field strength to induce the multiphoton excitation without damaging the fused silica system since it contains only 1.5 field cycles. Moreover, our pump pulse spans over 1.5 octaves, allowing for multiphoton excitation of fused silica with different photon combinations from the UV, Visible, and NIR spectral regions. Also, the short pulse duration of the pump pulse (2.7 fs) implies that all the photons in the pump pulse are almost in phase, which is a key for inducing the reflectivity switching in the sub-femtosecond time scale. Note, the weak intensity optical pulse (at the same level as our probe pulse intensity) will not induce the multiphoton excitation, thus no temporally oscillation or reflectivity modulation would be observed.

Additionally, the presented reflectivity modulation spectrograms in Fig. 2a and b carries the signature of the broadband pump pulse spectral phase dispersion. Therefore, the presented experiment can be utilized as an accurate methodology for characterizing the ultrashort laser pulses and its spectral phase dispersion directly and with a high resolution (see Fig. S2b) which is beyond the capability of the typical ultrashort pulse characterization techniques (i.e., frequency-resolved optical gating). Moreover, this transient modification can be engineered by controlling the laser pulse waveform (spectral phase) to achieve a tunable refractive index of natural material (i.e., fused silica) by high intensity ultrashort lasers, which is only possible in metamaterials[35,36], opening the door for a vast range of applications in ultrafast photonics.

Ultrafast optical information encoding.

As demonstrated experimentally in Fig. 2, the light-induced phase transition of the fused silica allows us to switch between an ON and OFF state of the reflected light signal following the driver field. Consequently, the reflectivity modulation and the switching alterability can be controlled by tailoring the driver field waveform. Accordingly, we demonstrate next the control of the switching signals using on-demand complex synthesized waveforms generated by ALFS [4,32,37]. Figure 4a (I), b (I), and c (I), show some of the measured reflectivity modulation spectrograms—after subtracting background spectrum —triggered by three different synthesized light fields. The integrated intensities of the reflected spectra at different instances of time (above zero amplitude) are plotted in Fig. 4a (II), b (II), and c (II). Note, the light signal can also be measured by photodiode detector instead of the spectrometer to directly detect the integrated intensity signal. The light signal switches from ON to OFF states *uniformly* every half-cycle of the driver field. By setting a certain intensity amplitude threshold (60%) in Fig. 4a (II), b (II), and c (II)—which easily can be experimentally implemented or programmed in the photodetector —the number of the detected light signals (above this threshold) and the switching alternative-time varies depending on the shape of the driver waveform. Figure 4a (III), b (III), and c (III) show the signals above the 60% threshold, and the insets in the top (contains 22 slots) represent the signal status (OFF or ON) in black and white in real-time at each half cycle of the driver field. Using the first waveform, the signal switches ON and OFF three times with a time separation of 4.5 fs and 3.6 fs. This switching time interval is controlled to be 3.6 and 1.8 fs (as shown in Fig. 4b(II)) using the second waveform. Moreover, the number of the switching signal increases to four by using the third waveform with 1.8, 1.8, and 3.6 fs time period separations between the signals as shown in Fig. 4c (III).

Remarkably, this capability of controlling the light signal switching (ON/OFF) allows the ultrafast data encoding with synthesized light waveforms[32], which are beyond the reach of conventional ultrafast pulses field. Accordingly, the reflected signal above the threshold will be detected “ON status” and presents the binary code “1”. The reflected signal below the threshold— will not be detected by the photodetector and hence will have an “OFF status”— representing the binary code “0”. The number of coding bits that the light field can carry equals twice of the number of the driver light field cycles. Some of the examples of binary encoding using the synthesized waveforms are shown in the insets of Fig. 4a (III), b (III), and c (III). Remarkably, the presented experiments are conducted in ambient conditions at room temperature which promises viable engineering of the demonstrated light field encoding to stabilize the long-anticipated ultrafast photonics.

In a potential ultrafast light field encoding process (illustrated in Fig. S3), the data will be encoded on the synthesized light waveforms generated by the ALFS[32] (or any pulse shaping device), which will act as an "encoder" device. Then, the synthesized waveform (which is considered to be the encoded laser beam) will carry the data from the transmitter to the receiver station. Next, the encoded laser beam will be focused on the dielectric together with another beam (decoder laser beam). Finally, the reflected decoder laser beam from the dielectric will be detected by a photodetector. After setting a certain predefined threshold, the photodetector will read the coded data in the 1 & 0 binary form. The light field encoding can

be obtained using multicycle pulses, which are provided by the commercial laser systems available in the market, in combination with pulse shaping and light field synthesis technology[3,4,32,37–39]. Notably, this demonstrated optical switching occurs in ambient conditions allowing a simple realistic architecture of a potentially realistic compact optical switch integrated on a photonic chip. Moreover, the data encoding on ultrafast light waveforms, in contrast to the encoding provided by modern electronic sources using a microwave, would significantly enhance the data processing and transformation speed for light-time distances.

In conclusion, the light-field induced phase transition of dielectric system in strong field enables switching the reflected light signal ON and OFF with attosecond switching speed. The light field tailoring and shaping with high resolution allow us to demonstrate the attosecond optical switching control and data binary encoding by synthesized laser pulses. This work paves the way to develop an ultrafast optical-based switches, and to transfer data with petahertz speed and beyond, which can carry information to the deep space opening a new era in communication and information technology.

Materials & Method

Time-resolved reflected spectra measurements

A multicycle pulse carried at a central wavelength of 800 nm is focused and propagated in a Hollow-Core-Fiber (HCF) to generate a broadband spectrum that spans from Ultra-Violet (UV) to Near-Infrared (NIR) spectral regions. This supercontinuum is divided into three spectral channels and compressed inside the attosecond light field synthesizer (ALFS) apparatus[32]. At the exist of ALFS, the three channels are superimposed to generate a synthesized waveform of 2.7 fs pulse. The relative delays and intensities of the three channels inside the ALFS are controlled to synthesize complex waveforms on-demand. The carrier-envelope-phase of the synthesized waveform is passively locked to less than 100 mrad (the laser source is OPCPA based). Also, the relative phases between the three channel's pulses inside the ALFS are actively locked to ensure the waveform stability during the experiment[32]. The output beam from the ALFS is divided into two beams by passing through a two-hole mask with different hole diameters. One of the two merged beams, has a high intensity (estimated field strength is 1 V/Å), is utilized as a pump beam to alter the reflectivity of the dielectric system[9]. The second beam (probe beam) has a lower intensity (~ 2.5% of the pump beam intensity) so it is not inducing any reflectivity changes on the system. Notably, the pump and probe pulses have the same waveforms (merged from one input pulse). The two beams are focused and overlapped on the fused silica sample (thickness ~ 100) by two focusing D-shape mirrors (f = 10 cm). One of the two D-shape mirrors is attached to a high-resolution (nanometer) delay stage. The probe beam is partially reflected from the fused silica sample, then it is filtered out from the pump beam, and focused on the entrance of an optical spectrometer. The reflected probe beam's spectra are acquired as a function of the time delay between the pump and probe pulses. Moreover, The complex waveforms used to control the reflectivity and control the switching signals (shown in Fig. 4) are generated by changing the relative phase delay and intensities between the ALFS channels, more details

about the light field synthesis scheme by ALFS can be found elsewhere[32]. Moreover, the sampling of the arbitrary waveforms utilized in the demonstration of the light field encoding experiments is performed with the same setup and at the same light field sampling position. Worth mentioning, the potential photodiode for the ultrafast encoding applications shall have a high speed, and broad bandwidth response which covers from the DUV to NIR frequencies. Also, the photodiode should have a flat frequency response out to the whole spectral range of the probe light signal.

Declarations

Acknowledgments

This project is funded by the Gordon and Betty Moore Foundation Grant **GBMF7938** to M. Hassan. This material is also based upon work supported by the Air Force Office of Scientific Research under award number **FA9550-19-1-0025**.

Author Contributions:

D.H. and H.A conducted the experiments and analyzed the data. S.Z. and E.C. carried out the simulations and calculations. V.P. designed and measured the optics of the ALFS. M.H. conceived, supervised, and directed the study. All authors discussed the results and their interpretation and wrote the manuscript.

Ethics declarations

Authors declare no competing interests.

Data Availability

The datasets generated and/or analyzed during this study are available from the corresponding authors on reasonable request.

Code availability

The analysis codes that support the study's findings are available from the corresponding authors on reasonable request.

References

1. Krausz, F. & Ivanov, M. Attosecond physics. Rev. Mod. Phys. **81**, 163, (2009).
2. Corkum, P. & Krausz, F. Attosecond science. Nature Physics **3**, 381–387, (2007).
3. Wirth, A. *et al.* Synthesized Light Transients. Science **334**, 195–200, (2011).
4. Hassan, M. T. *et al.* Optical attosecond pulses and tracking the nonlinear response of bound electrons. Nature **530**, 66–70, (2016).

5. Ghimire, S. *et al.* Observation of high-order harmonic generation in a bulk crystal. Nature physics **7**, 138–141, (2011).
6. Schiffrin, A. *et al.* Optical-field-induced current in dielectrics. Nature **493**, 70–74, (2013).
7. Schultze, M. *et al.* Controlling dielectrics with the electric field of light. Nature **493**, 75–78, (2013).
8. Luu, T. T. *et al.* Extreme ultraviolet high-harmonic spectroscopy of solids. Nature **521**, 498–502, (2015).
9. Hui, D. *et al.* Attosecond electron motion control in dielectric. Nature Photonics **16**, 33–37, (2022).
10. Alqattan, H., Hui, D., Sennary, M. Y. S. & Hassan, M. Attosecond electronic delay response in dielectric materials. Faraday Discussions, (2022).
11. Apalkov, V. & Stockman, M. I. Theory of dielectric nanofilms in strong ultrafast optical fields. Physical Review B **86**, 165118, (2012).
12. Wachter, G. *et al.* Ab initio simulation of electrical currents induced by ultrafast laser excitation of dielectric materials. Physical review letters **113**, 087401, (2014).
13. Glezer, E., Siegal, Y., Huang, L. & Mazur, E. Laser-induced band-gap collapse in GaAs. Physical Review B **51**, 6959, (1995).
14. Khurgin, J. B. Optically induced currents in dielectrics and semiconductors as a nonlinear optical effect. JOSA B **33**, C1-C9, (2016).
15. Paasch-Colberg, T. *et al.* Sub-cycle optical control of current in a semiconductor: from the multiphoton to the tunneling regime. Optica **3**, 1358–1361, (2016).
16. Sederberg, S. *et al.* Attosecond optoelectronic field measurement in solids. Nature communications **11**, 1–8, (2020).
17. Korobenko, A. *et al.* Femtosecond streaking in ambient air. Optica **7**, 1372–1376, (2020).
18. Yabana, K., Sugiyama, T., Shinohara, Y., Otobe, T. & Bertsch, G. Time-dependent density functional theory for strong electromagnetic fields in crystalline solids. Physical Review B **85**, 045134, (2012).
19. Ono, M. *et al.* Ultrafast and energy-efficient all-optical switching with graphene-loaded deep-subwavelength plasmonic waveguides. Nature Photonics **14**, 37–43, (2020).
20. Zasedatelev, A. V. *et al.* A room-temperature organic polariton transistor. Nature Photonics **13**, 378–383, (2019).
21. Nozaki, K. *et al.* Sub-femtojoule all-optical switching using a photonic-crystal nanocavity. Nature Photonics **4**, 477–483, (2010).
22. Yang, Y. *et al.* Femtosecond optical polarization switching using a cadmium oxide-based perfect absorber. Nature Photonics **11**, 390–395, (2017).
23. Li, W. *et al.* Ultrafast all-optical graphene modulator. Nano letters **14**, 955–959, (2014).
24. Takahashi, R., Itoh, H. & Iwamura, H. Ultrafast high-contrast all-optical switching using spin polarization in low-temperature-grown multiple quantum wells. Applied Physics Letters **77**, 2958–2960, (2000).

25. Tan, W., Ma, J., Zheng, Y. & Tong, J. Femtosecond optical Kerr gate with double gate pulses. IEEE Photonics Technology Letters **30**, 266–269, (2017).
26. Liu, Y. *et al.* 10 fs ultrafast all-optical switching in polystyrene nonlinear photonic crystals. Applied Physics Letters **95**, 131116, (2009).
27. Hirao, K., Mitsuyu, T., Si, J. & Qiu, J. *Active glass for photonic devices: photoinduced structures and their application*. Vol. 7 (Springer Science & Business Media, 2013).
28. Iizuka, N., Kaneko, K. & Suzuki, N. All-optical switch utilizing intersubband transition in GaN quantum wells. IEEE journal of quantum electronics **42**, 765–771, (2006).
29. Sethi, P. & Roy, S. All-optical ultrafast XOR/XNOR logic gates, binary counter, and double-bit comparator with silicon microring resonators. Applied optics **53**, 6527–6536, (2014).
30. Zhang, Q. *et al.* Ultrafast optical Kerr effect of Ag–BaO composite thin films. Applied physics letters **82**, 958–960, (2003).
31. Li, Y., Bhattacharyya, A., Thomidis, C., Moustakas, T. D. & Paiella, R. Ultrafast all-optical switching with low saturation energy via intersubband transitions in GaN/AlN quantum-well waveguides. Optics Express **15**, 17922–17927, (2007).
32. Alqattan, H., Hui, D., Pervak, V. & Hassan, M. T. Attosecond light field synthesis. APL Photonics **7**, 041301, (2022).
33. Tritschler, T., Mücke, O., Wegener, M., Morgner, U. & Kärtner, F. Evidence for third-harmonic generation in disguise of second-harmonic generation in extreme nonlinear optics. Physical review letters **90**, 217404, (2003).
34. Luo, C.-W., Wang, Y., Chen, F., Shih, H. & Kobayashi, T. Eliminate coherence spike in reflection-type pump-probe measurements. Optics express **17**, 11321–11327, (2009).
35. Boardman, A. D. *et al.* Active and tunable metamaterials. Laser & Photonics Reviews **5**, 287–307, (2011).
36. Landy, N. I., Sajuyigbe, S., Mock, J. J., Smith, D. R. & Padilla, W. J. Perfect metamaterial absorber. Physical review letters **100**, 207402, (2008).
37. Hassan, M. T. *et al.* Invited Article: Attosecond photonics: Synthesis and control of light transients. Review of Scientific Instruments **83**, 111301, (2012).
38. Weiner, A. M. Ultrafast optical pulse shaping: A tutorial review. Optics Communications **284**, 3669–3692, (2011).
39. Cundiff, S. T. & Weiner, A. M. Optical arbitrary waveform generation. Nature Photonics **4**, 760–766, (2010).

Figures

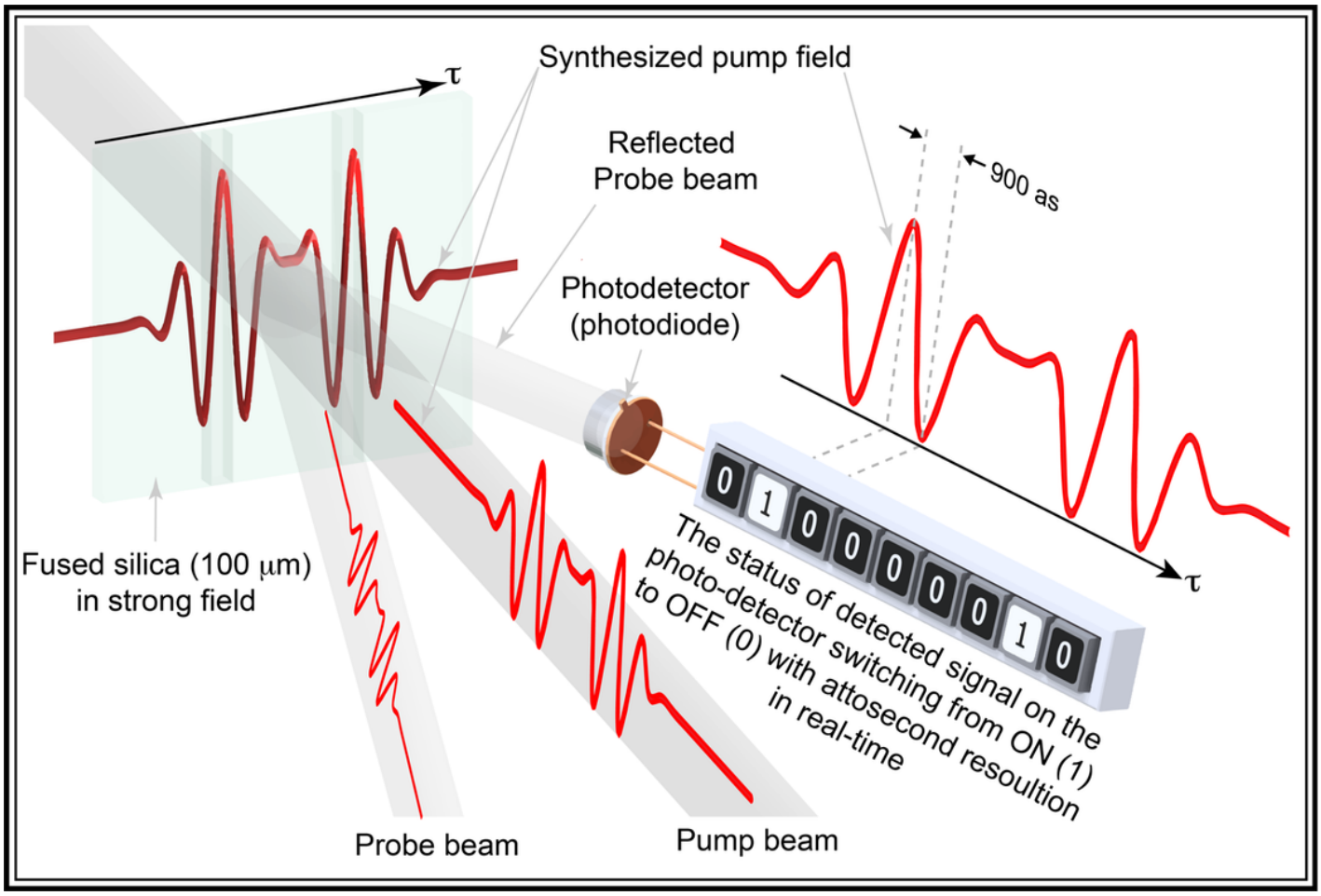

Figure 1

The basic principle of the attosecond optical switching based on strong field interaction with dielectric. The pump light field induces the instantaneous phase transition in the dielectric (fused silica) system and causes the change in the reflectivity of the dielectric following the shape of the incident pump pulse waveform in real-time. The reflectivity modification is detected by measuring the reflected probe beam's change using a photodetector (e.g., photodiode) as a function of the time delay between pump and probe beams. The detected reflected signal is switched OFF/ON (presented by 0/1), depending on the field intensity at the time τ, in the real-time. The switching resolution is equal to the duration of the half-cycle field (900 as) of the pump pulse and can be controlled by tailoring the pump field waveform using the attosecond light field synthesis approach. The attosecond optical switching and control allow to encode data on ultrafast laser pulse and open the door for establishing the ultrafast optical switches.

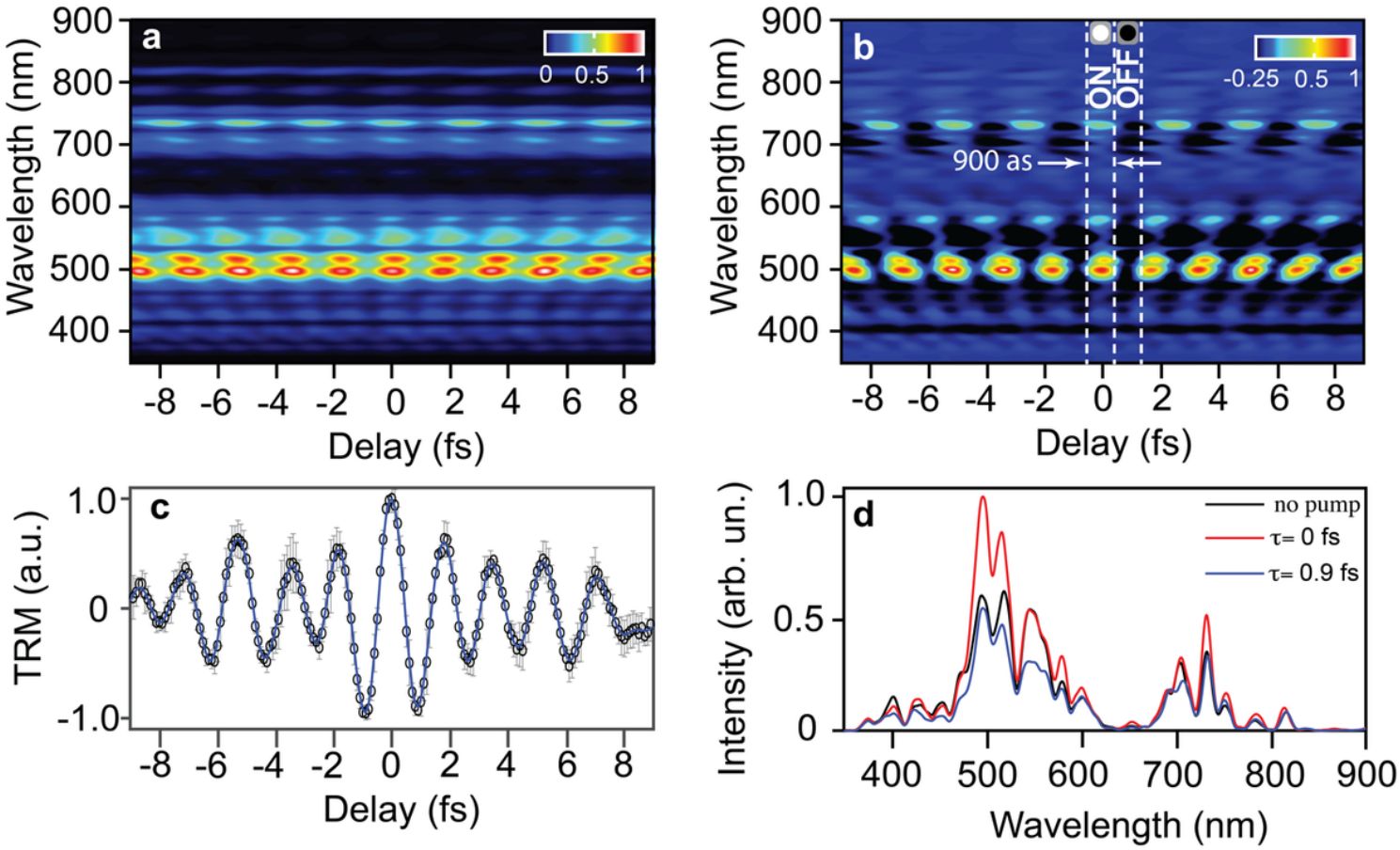

Figure 2

Attosecond optical switching. The reflectivity of SiO_2 is modulated in real-time due to the interaction with a strong (pump) light field. **a**, The measured spectrogram (average three scans) of the reflected probe beam as a function of the time delay between the pump and probe pulses. **b**, The obtained spectrogram by subtracting the probe spectrum in the absence of pump field from the measured spectrogram (shown in a). The reflectivity switches between maximum to minimum alternatively in 900 attosecond time scale. **c**, The normalized total reflectivity modulation (TRM) of the SiO_2 in the strong field retrieved obtained from the measured spectrogram (in a) by the integration of the probe spectrum at each instance of time. **d**, The probe beam's spectrum reflected from the SiO_2 in the equilibrium state (in the absence of pump field) is shown in the black line. In contrast, reflected spectra intensities of the probe beam (outlined from the spectrogram in **a)** at τ=0 & 0.9 fs are plotted in red and blue lines, respectively.

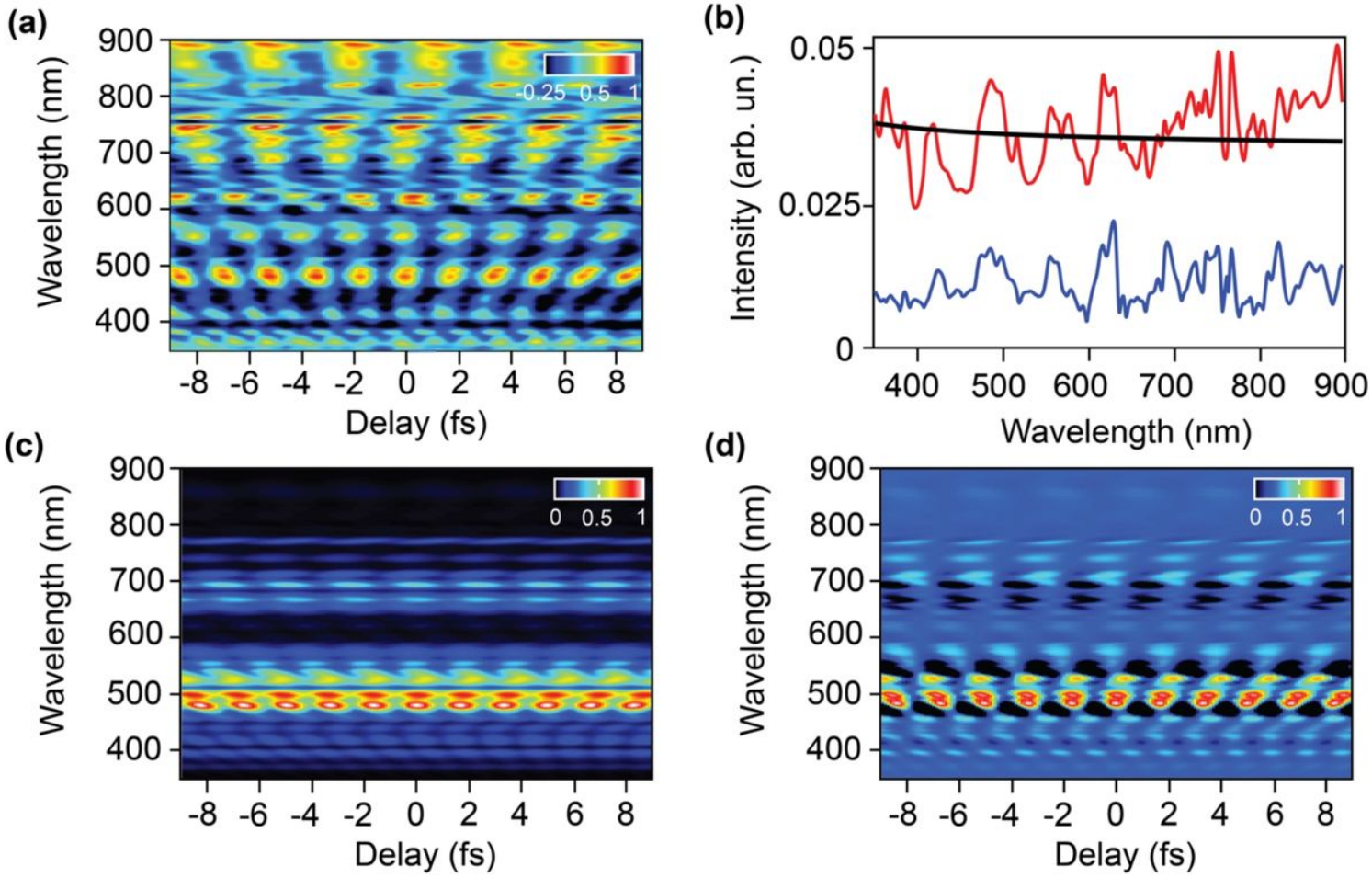

Figure 3

Simulated reflectivity dynamics of fused silica in a strong light field. a, The retrieved reflectivity behavior of fused silica in strong field extracted from the measured spectrogram (see text) in frequency and time domains. **b**, The amplitude of the reflectivity oscillation as a function of wavelength is shown in blue line calculated by halving the difference between maximum and minimum of an oscillation cycle. The offset is calculated by averaging the maximum and minimum in an oscillation cycle and shown in red line. The transient reflectivity change of SiO_2 under no influence of the pump pulse is shown in black line. **c &d,** The simulation of the measured spectrograms in Fig. 2b&c, respectively, calculated by the developed simple model considering the effect of the spectral phase of the driver pulse as explained in the text.

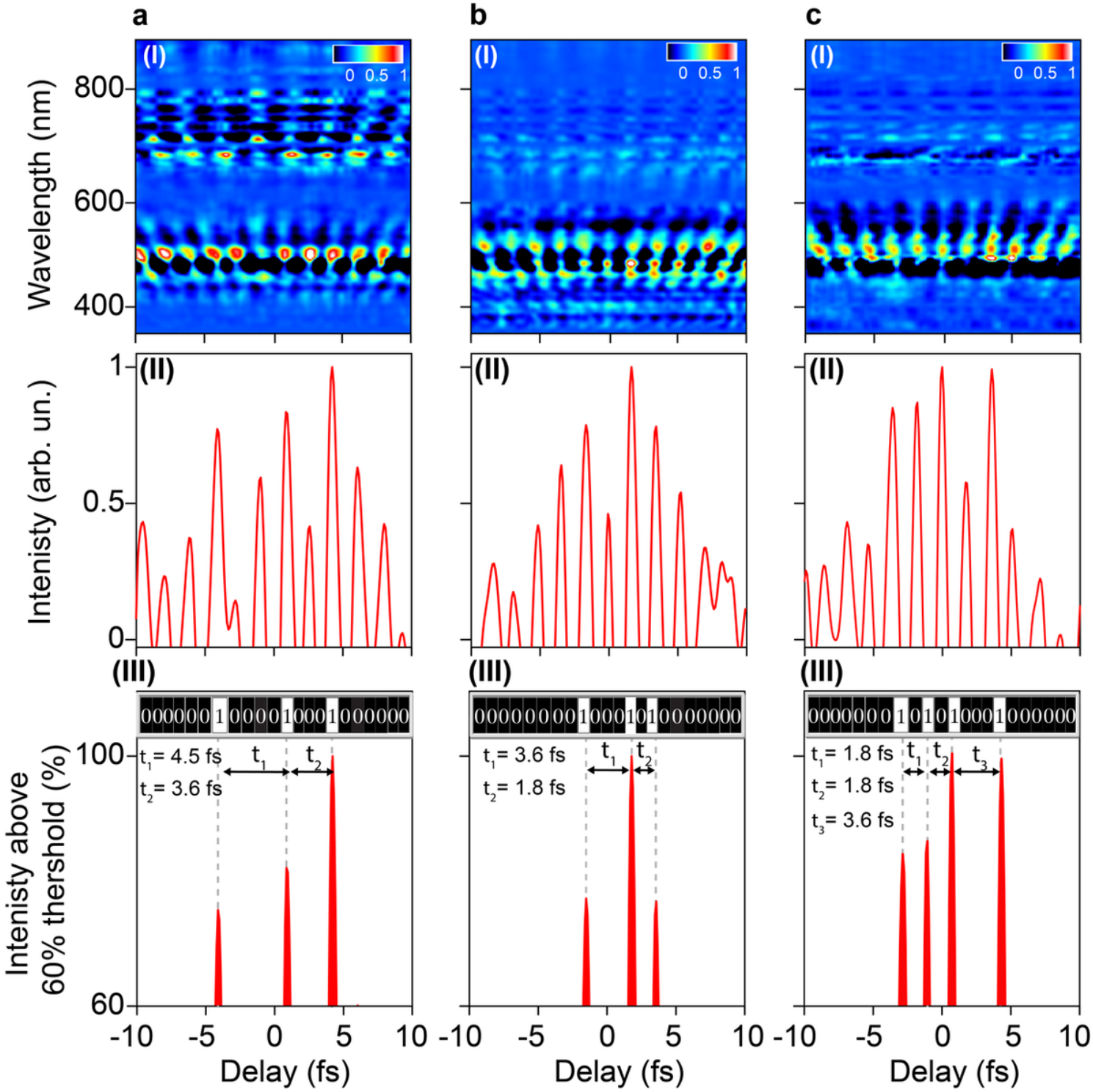

Figure 4

Ultrafast light field encoding. a (I), b (I), c (I), The measured spectrograms of the reflected probe beam triggered by three different synthesized waveforms after subtracting the probe spectrum in the absence of the pump field. **a (II), b (II), c (II),** The positive value of the probe spectra integration as a function of time, representing the measured light signal by a photodetector in real-time, after subtracting the background. The light signal switches ON/OFF alternatively every half-cycle**. a (III), b (III), c (III),** The detected light signals above a 60% threshold. The light signals are switched ON and OFF at different time

intervals. In the insets, the slots presenting the signal detection status in real-time as follows: black (0) means no signal detected above the threshold, while white (1) means the signal is above the threshold and seen by the detector. This optical switching signal control would enable the binary data encoding on light fields with petahertz speed.

Supplementary Files

This is a list of supplementary files associated with this preprint. Click to download.

- AttosecondOpticalSwitchingSI.docx